# ZnO Metal-Semiconductor-Metal Ultraviolet Photodiodes with Au Contacts

## S. J. Young,[a] L. W. Ji,[b] S. J. Chang,[a,z] and X. L. Du[c]

[a]*Institute of Microelectronics and Department of Electrical Engineering, National Cheng Kung University, Tainan 70101, Taiwan*
[b]*Institute of Electro-Optical and Materials Science, National Formosa University, Yunlin 632, Taiwan*
[c]*Institute of Physics, Chinese Academy of Sciences, Beijing 100080, China*

ZnO epitaxial films were grown on (0001) sapphire substrates by radio-frequency plasma-assisted molecular beam epitaxy. Au/ZnO/Au metal-semiconductor-metal ultraviolet photodiodes with various finger widths and pitches ranging from 10 to 30 $\mu$m were also fabricated. It was found that we achieved largest detector responsivity from the $10 \times 10$ photodiodes with 10 $\mu$m finger width and 10 $\mu$m pitch. It was also found that the responsivity increases with the applied bias. With an incident wavelength of 370 nm and 1 V applied bias, it was found that the responsivity for the $10 \times 10$ photodiode was 0.135 A/W, which corresponds to a quantum efficiency of 44.9%. Furthermore, it was found that noise equivalent power and corresponding detectivity $D^*$ of the $10 \times 10$ photodiodes were $3.17 \times 10^{-13}$ W and $2.23 \times 10^{12}$ cm Hz$^{0.5}$ W$^{-1}$, respectively.
© 2006 The Electrochemical Society. [DOI: 10.1149/1.2387058] All rights reserved.

In recent years, much research has been focused on semiconductor-based ultraviolet (UV) photodiodes.[1] Photodiodes operating in UV region are important devices that can be used in various commercial and military applications. For example, visible-blind UV photodiodes can be used in space communications, ozone layer monitoring, and flame detection. Currently, light detection in UV spectral range still uses Si-based optical photodiodes. Although Si-based photodiodes are sensitive to visible and infrared radiation, the responsivity in UV region is low as room-temperature bandgap energy of Si is only 1.2 eV. With the advent of optoelectronic devices fabricated on wide direct band gap materials, it becomes possible to produce high-performance solid-state photodiodes that are sensitive in the UV region. For example, GaN-based UV photodiodes are already commercially available.[2,3] ZnSe-based UV photodiodes have also been demonstrated.[4]

ZnO is another wide direct bandgap material that is sensitive in the UV region.[5,6] The large exciton binding energy of 60 meV and wide bandgap energy of 3.37 eV at room temperature make ZnO a promising photonic material for applications such as light-emitting diodes, laser diodes, and UV photodiodes. Indeed, ZnO has attracted much attention in recent years.[7-9] High-quality ZnO epitaxial layers can be grown by metallorganic chemical vapor deposition,[5] molecular beam epitaxy (MBE),[10] and pulsed laser deposition[11] on top of ZnO substrates,[6] sapphire substrates,[12] and epitaxial GaN layers.[13] ZnO Schottky diodes and metal-semiconductor-metal (MSM) photodiodes detecting in UV region have also been demonstrated.[8] MSM photodiodes consist of two interdigitated Schottky contacts deposited on top of an active layer. The reduced parasitic capacitance of this structure, as well as the low dark current and noise values, and its linearity with optical power, make MSM detectors the most promising candidates for high-speed photodetection.[14-16] To achieve high-performance MSM UV photodiodes, it is important to improve crystal quality and to achieve large Schottky barrier height at metal-semiconductor interface. A large barrier height leads to small leakage current and high breakdown voltage which could result in improved responsivity and photocurrent to dark current contrast ratio. To achieve a large Schottky barrier height on ZnO, one can choose metals with high work functions.[17] However, many of the high work function metals are not stable at high temperatures. In other words, severe interdiffusion might occur at the metal-ZnO interface. In addition, further progress can be achieved by optimizing the processing or the design. In this work, we report the growth of ZnO epitaxial layers by MBE and the fabrication of ZnO-based MSM photodiodes with various finger widths and pitches. The noise behavior of the fabricated ZnO MSM photodiodes is also discussed.

## Experimental

Samples used in this study were all grown by radio-frequency (rf) plasma-assisted MBE (Omni Vac) on sapphire (0001) substrates. The base pressure in the growth chamber was $\sim 1.4 \times 10^{-11}$ Pa. The source material of Zn was elemental Zn (6N) evaporated from a commercial Knudsen cell (Crea Tech). Active oxygen and nitrogen radicals were separately produced by two rf-plasma systems (SVTA). The flow rate of oxygen/nitrogen gas was controlled by a mass flow controller (ROD-4, Aera). Prior to the growth, we first degreased sapphire substrates in trichloroethylene and acetone. These sapphire substrates were then etched in $H_2SO_4$:$H_3PO_4$ = 3:1 at 110°C for 30 min followed by rinsing in deionized water. The sapphire substrates were then loaded into the growth chamber. We then exposed the sapphire substrates to oxygen radicals for 30 min at 180°C with 350 W rf power and 2.5 sccm oxygen flux so as to form oxygen-terminated sapphire surface. After this treatment, we exposed the sapphire substrates to nitrogen radicals for 1 h at 180°C with 480 W rf power and 3.0 sccm nitrogen flux for nitridation. When ZnO is directly grown on Al monolayer-terminated surface, inversion domains are inevitably introduced to the ZnO epilayer due to the coexistence of Al sublattice and O sublattice on this surface. Note that the formation of a uniform O-terminated surface prior to nitridation is crucial for the formation of the N-polar AlN and the suppression of the Zn-polar inversion domains. Note also that nitridation involves the diffusion of nitrogen atoms into sapphire and the substitution for oxygen. We can thus achieve N-polar AlN thin layer due to atom substitution[18] and subsequently achieve high-quality unipolar single-domain ZnO films. From the reflection high energy electron diffraction patterns, it was found that a very thin AlN layer ($\sim 2$ nm) was formed with a 30° in-plane rotation of its lattice with respect to that of sapphire substrates after nitridation. We subsequently grew a 1000 nm thick unintentionally doped ZnO epitaxial layer with conventional two-step growth method, i.e., a low-temperature buffer layer grown at 400°C, and a high-temperature layer grown at 650°C. After the growth, we in situ annealed the ZnO epitaxial layer at 750°C. At this moment, we observed $3 \times 3$ reconstruction pattern which indicates O-polar of our ZnO films.[19] From room-temperature Hall measurements, it was found that carrier concentration and mobility of the as-grown ZnO films were 1.71 $\times 10^{16}$ cm$^{-3}$ and 26.4 cm$^2$/V s, respectively. The low mobility observed from our ZnO epitaxial layers should directly relate to the large lattice mismatch between ZnO and the underneath sapphire
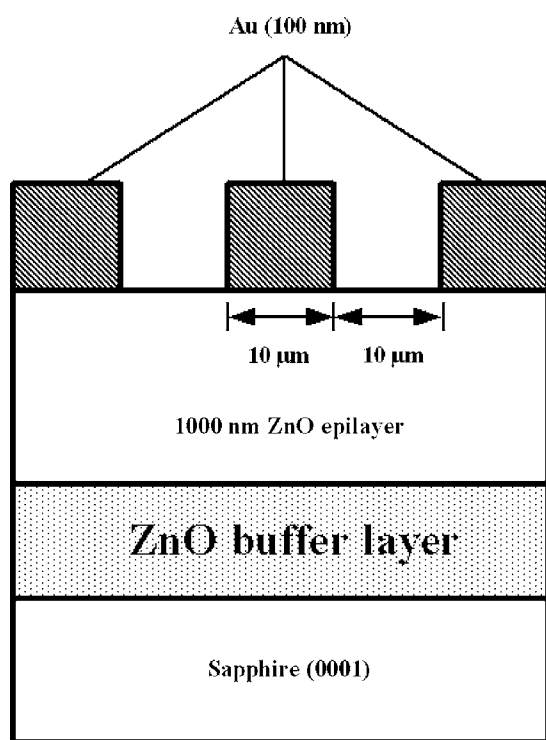
z E-mail: changsj@mail.ncku.edu.tw

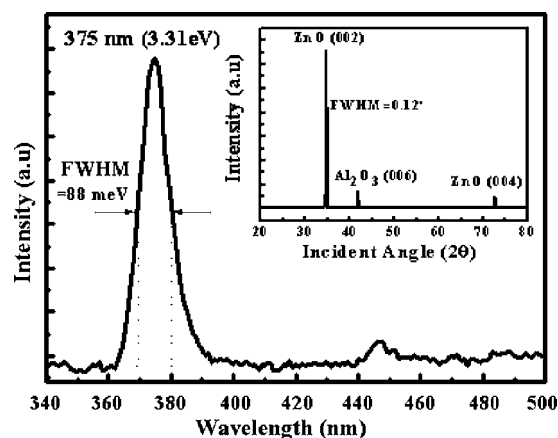**Figure 1.** Structure of ZnO MSM photodiode with Au contacts.



**Figure 2.** Room-temperature PL spectrum of epitaxial ZnO films. The inset shows XRD spectrum of the epitaxial ZnO films prepared on sapphire substrate.

substrates. Room-temperature photoluminescence (PL) and X-ray diffraction (XRD) measurements were also performed to evaluate quality of the as-grown samples.

MSM photodiodes with various finger widths and pitches were then fabricated. We first cleaned the ZnO samples by acetone and methanol. 100 nm thick Au film was subsequently deposited onto the sample surface by E-gun evaporation to serve as metal contacts. Standard lithography and etching were then performed to define the interdigitated contact pattern. All the devices have an active area of $200 \times 200 \ \mu m$. The schematic structure of the ZnO MSM photodetectors with 10 $\mu$m finger width and spacing is shown in Fig. 1. Photocurrent and dark current of the fabricated photodiodes were then measured by an HP4145B semiconductor parameter analyzer. Spectral responsivity measurements were also performed using a 250 W xenon arc lamp light source and a monochromator. Low-frequency noises of the fabricated photodetectors were also measured in the frequency range of 1 Hz to 100 kHz using a low noise current preamplifier and an HP35670A fast Fourier transform spectrum analyzer.

## Results and Discussion

Figure 2 shows room-temperature PL spectrum of our ZnO epitaxial films. It was found that we observed a strong excitonic related PL peak at 375 nm (3.31 eV) and a very weak green band emission at around 450 nm. The green luminescence band is originated from oxygen vacancy related defects. It was also found that full-width-half-maximum (fwhm) of the excitonic related PL peak was only 88 meV.[12] Furthermore, it was found that the intensity ratio between excitonic band emission and green band emission was extremely large. These results all indicate good crystal quality of our ZnO epitaxial layers.[12] The inset in Fig. 1 shows measured XRD spectrum of the 1000 nm thick ZnO epitaxial film prepared on sapphire substrate. The peak occurred at $2\theta = 41.9°$ in the spectrum was originated from the (006) plane of sapphire substrate. We also observed a ZnO (002) XRD peak at $2\theta = 34.3°$ with a fwhm of 0.12°. Such a result indicates that the ZnO film was preferentially grown in

*c*-axis direction. The small fwhm of the ZnO(002) XRD peak again indicates good crystal quality of our samples.

Figure 3 shows current-voltage (*I-V*) characteristics of the fabricated ZnO MSM photodiodes with various finger widths and pitches measured in dark (dark current) and under 370 nm illumination (photocurrent). The dark current is originated from thermionic and field emission of carriers. With the same applied bias, it was found that we achieved the highest dark current from the $10 \times 10$ photodiode with the smallest finger width (i.e., 10 $\mu$m) and pitch (i.e., 10 $\mu$m). This could be attributed to the largest electrical field induced in the photodiode with the smallest finger widths and pitches. Again, it was found that we achieved the largest photocurrent from the $10 \times 10$ photodiode with the smallest finger width and pitch.

Photocurrent to dark current contrast ratios for the fabricated photodiodes can also be determined from the measured dark currents and photocurrents, as shown in the insert in Fig. 3. With 5 V applied bias, it was found that photocurrent to dark current contrast ratios were 5790, 187, and 17.5 for the $10 \times 10$, $20 \times 20$, and $30 \times 30$ ZnO MSM photodiodes, respectively. These values indicate that the reduction of the finger width and pitch enhances the photocurrent to dark current contrast ratios of our ZnO MSM photodiodes. Figure 4 shows measured optical responsivity of the fabricated photodiodes. It was found that we achieved larger detector responsivity from the photodiodes with smaller finger width and
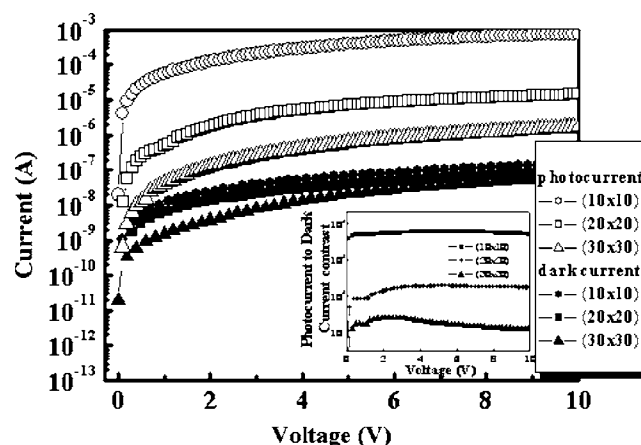


**Figure 3.** *I-V* characteristics of the ZnO MSM photodiodes measured in the dark and under illumination. The inset shows photocurrent to dark current contrast ratios.
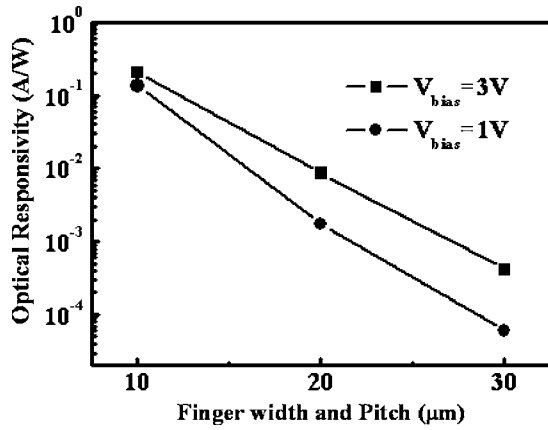
**Figure 4.** Influence of the finger width and pitch distance in the optical responsivity, for two different $V_{bias}$.



**Figure 6.** Low-frequency noise spectra of the $(10 \times 10)$ Au/ZnO/Au MSM photodiodes.

pitch. It was also found that the responsivity increases with the applied bias. Figure 5 shows measured spectral responsivities of the $10 \times 10$ ZnO MSM photodiodes. As shown in Fig. 5, it was found that the photodiode responsivities were nearly constants in the below bandgap UV region while sharp cutoffs with a drop of three orders of magnitude occurred at ~370 nm. With an incident wavelength of 370 nm and 1 V applied bias, it was found that the maximum responsivity for the fabricated photodiodes was 0.135 A/W, which corresponds to a quantum efficiency of 44.9%.

Figure 6 shows low-frequency noise spectra of the $10 \times 10$ ZnO MSM photodiodes with Au electrodes. From these curves, it was found that measured noise power densities, $S_n(f)$, could be fitted well by $1/f^\gamma$ with $\gamma = 1$. The observed pure $1/f$ noise indicates that trapping states are distributed uniformly in energy for the device. For a given bandwidth of B, we could estimate the total square noise current by integrating $S_n(f)$ over the frequency range

$$\langle i_n \rangle^2 = \int_0^B S_n(f)df = \int_0^1 S_n(1)df + \int_1^B S_n(f)df = S_0[1 + \ln(B)]$$

[1]

where $S_n(f)$ in the bandwidth range from 0 to 1 was assumed to be the same and equals to $S_0$ [$S_n(f)$ at 1 Hz]. Thus, the noise equivalent power (NEP) can be given by
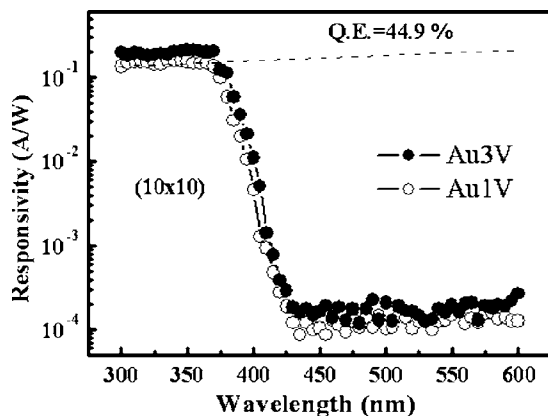
$$NEP = \frac{\sqrt{\langle i_n \rangle^2}}{R}$$

[2]

where $R$ is the responsivity of the photodiodes. The normalized detectivity, $D^*$, could then be determined by

$$D^* = \frac{\sqrt{A}\sqrt{B}}{NEP}$$

[3]

where **A** and **B** are the area of the photodiode and the bandwidth, respectively. For a given bandwidth of 100 Hz and a 1 V applied bias, we found that NEP and corresponding detectivity $D^*$ of our Au/ZnO/Au MSM photodiodes were $3.17 \times 10^{-13}$ W and $2.23 \times 10^{12}$ cm Hz$^{0.5}$ W$^{-1}$, respectively. Note that the value of $D^*$ measured from the fabricated photodiodes were higher than that observed from other GaN-based and ZnSe MSM photodiodes.[20,21] Such a result suggests ZnO is potentially useful for UV detector applications. As shown in Fig. 7, it was found that NEP increased and $D^*$ decreased monotonically with the applied bias. This is because the increase in responsivity is much smaller than the increase of total noise power density as the applied bias is increased for our photodiodes. Thus, NEP and $D^*$ of our photodiodes were both dominated by the total noise power density. The insert plot in Fig. 7 shows noise power density as a function of dark current for the fabricated photodiodes measured at 100 Hz. It was found that mea-



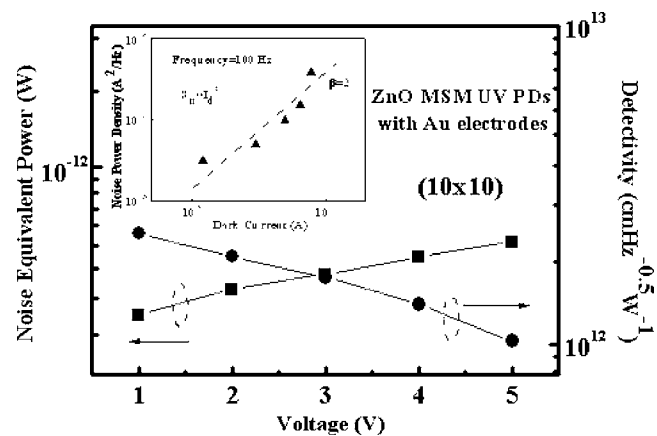**Figure 5.** Measured spectral responsivites of the $(10 \times 10)$ fabricated Au/ZnO/Au MSM photodiodes.



**Figure 7.** NEP and detectivity as a function of applied voltage of the $(10 \times 10)$ ZnO MSM UV photodiodes. The inset plot shows noise power densities as a function of dark current measured at 100 Hz.

sured noise power densities could be fitted well by the following equation.

$$S_n(f) = K\left(\frac{I_d^{\beta}}{f^{\gamma}}\right) \qquad [4]$$

where $S_n(f)$ is the spectral density of the noise power, $K$ is a constant, $I_d$ is the dark current, $\beta$ and $\gamma$ are two fitting parameters. From Fig. 7, it was found that $\beta$ and $\gamma$ were 2 and 1, respectively. Such a result agrees well with Kleinpenning's model that spectral density of $1/f$ noise should proportional to $I_d^2$.[22] In other words, $1/f$ noise induced increase in current is related to the modulation of Schottky barrier height by uniformly distributed trapping states in our photodetectors.

## Conclusions

ZnO epitaxial films were grown on sapphire substrates by MBE. Au/ZnO/Au MSM UV photodiodes with various finger widths and pitches ranging from 10 to 30 $\mu$m were also fabricated. It was found that we achieved largest detector responsivity from the $10 \times 10$ photodiodes with 10 $\mu$m finger width and 10 $\mu$m pitch. It was also found that the responsivity increases with the applied bias. With an incident wavelength of 370 nm and 1 V applied bias, it was found that the responsivity for the $10 \times 10$ photodiode was 0.135 A/W, which corresponds to a quantum efficiency of 44.9%. Furthermore, it was found that NEP and corresponding detectivity $D^*$ of the $10 \times 10$ photodiodes were $3.17 \times 10^{-13}$ W and $2.23 \times 10^{12}$ cm Hz$^{0.5}$ W$^{-1}$, respectively.

## Acknowledgments

## References

1. M. Razeghi and A. Rogalski, *J. Appl. Phys.*, **79**, 7473 (1996).
2. Y. K. Su, S. J. Chang, C. H. Chen, J. F. Chen, G. C. Chi, J. K. Sheu, W. C. Lai, and J. M. Tsai, *IEEE Sens. J.*, **2**, 366 (2002).
3. Y. Z. Chiou, *J. Electrochem. Soc.*, **152**, G639 (2005).
4. S. J. Chang, T. K. Lin, Y. K. Su, Y. Z. Chiou, C. K. Wang, S. P. Chang, C. M. Chang, J. J. Tang, and B. R. Huang, *Mater. Sci. Eng., B*, **127**, 164 (2006).
5. T. M. Barnes, J. Leaf, S. Hand, C. Fry, and C. A. Wolden, *J. Appl. Phys.*, **96**, 7036 (2004).
6. H. Kato, M. Sano, K. Miyanoto, and T. Yao, *Jpn. J. Appl. Phys., Part 1*, **42**, L1002 (2003).
7. Y. I. Alivov, E. V. Kalinina, A. E. Cherenkov, D. C. Look, B. M. Ataev, A. K. Omaev, M. V. Chukichev, and D. M. Bagnall, *Appl. Phys. Lett.*, **83**, 4719 (2003).
8. S. Liang, H. Sheng, Y. Liu, Z. Huo, Y. Lu, and H. Shen, *J. Cryst. Growth*, **225**, 110 (2001).
9. A. Mang, K. Reimann, and St. Rübenacke, *Solid State Commun.*, **94**, 251 (1995).
10. A. Setiawan, Z. Vashaei, M. W. Cho, T. Yao, H. Kato, M. Sano, K. Miyamoto, I. Yonenaga, and H. J. Ko, *J. Appl. Phys.*, **96**, 3763 (2004).
11. E. M. Kaidashev, M. Lorenz, H. von Wenckstern, A. Rahm, H. C. Semmelhack, K. H. Han, G. Benndorf, C. Bundesmann, H. Hochmuth, and M. Grundmann, *Appl. Phys. Lett.*, **82**, 3901 (2003).
12. K. Sakurai, D. Iwata, S. Fujita, and S. Fujita, *Jpn. J. Appl. Phys., Part 1*, **38**, 2606 (1999).
13. H. J. Ko, Y. F. Chen, S. K. Hong, and T. Yao, *J. Cryst. Growth*, **209**, 816 (2000).
14. R. P. Joshi, A. N. Dharamsi, and J. McAdoo, *Appl. Phys. Lett.*, **64**, 3611 (1994).
15. E. Monroy, F. Calle, J. L. Pau, E. Munõz, F. Omnès, B. Beaumont, and P. Gibart, *Phys. Status Solidi A*, **185**, 91 (2001).
16. J. C. Carrano, T. Li, P. A. Grudowski, C. J. Eiting, R. D. Dupuis, and J. C. Campbell, *J. Appl. Phys.*, **83**, 6148 (1998).
17. F. D. Auret, S. A. Goodman, M. Hayes, M. J. Legodi, H. A. van Laarhoven, and D. C. Look, *Appl. Phys. Lett.*, **79**, 3074 (2001).
18. Z. X. Mei, Y. Wang, X. L. Du, M. J. Ying, Z. Q. Zeng, H. Zheng, J. F. Jia, Q. K. Xue, and Z. Zhang, *J. Appl. Phys.*, **96**, 7108 (2004).
19. Y. F. Chen, H. J. Ko, S. K. Hong, and T. Yao, *Appl. Phys. Lett.*, **76**, 559 (2000).
20. C. K. Wang, S. J. Chang, Y. K. Su, Y. Z. Chiou, C. S. Chang, T. K. Lin, H. L. Liu, and J. J. Tang, *Semicond. Sci. Technol.*, **20**, 485 (2005).
21. F. Vigué, E. Tournié, and J. P. Faurie, *IEEE J. Quantum Electron.*, **37**, 1146 (2001).
22. T. G. M. Kleinpenning, *Solid-State Electron.*, **22**, 121 (1979).